



ESA cloud_cci

**Algorithm Theoretical Basis Document (ATBD) of the
Community Code for CLimate (CC4CL)
Broadband Radiative Flux Retrieval (CC4CL-TOAFLUX) module**

Version 1.1

Matthew W. Christensen^{1,2}, Caroline Poulsen¹, Greg McGarragh², and Roy G. Grainger²

¹Space Science and Technology Department, Rutherford Appleton Laboratory, Chilton, Didcot, OX11 0QX,
UK

²Atmospheric, Oceanic and Planetary Physics, University of Oxford, Oxford, OX1 3PU, UK

Questions concerning the document shall be addressed to

Matthew Christensen

Phone: 44-1235-446949

Email: matthew.christensen@stfc.ac.uk



Contents

1	Introduction	3
2	Algorithm	3
2.1	Description	3
2.2	Validation	5
2.3	Uncertainties	5
3	Science applications	6
3.1	Cloud & Aerosol Radiative Effects	6
4	Discussion and Summary	6
4.1	Future Algorithm Developments	7



1 Introduction

This document describes the implementation of the broadband radiative flux retrieval algorithm used in CC4CL (Community Code for CLimate). Broadband radiative fluxes are computed in a post-processing step of the cloud.CCI processor CC4CL using BUGSrad (Stephens et al., 2001). Top and bottom of atmosphere longwave and shortwave radiative fluxes are calculated using the cloud and aerosol properties retrieved from ORAC (Optimal Retrieval of Aerosol and Cloud). The ORAC scheme, applied to aerosol CCI (Climate Change Initiative) and Cloud_cci programmes, ensures a radiatively consistent set of cloud and aerosol retrieved properties because it performs the retrieval using all available instrument channels simultaneously. Documentation for the Cloud_cci program can be acquired online at <http://www.esa-cloud-cci.org>.

Accurate measurements of these fluxes are critical in order to quantify the radiative impacts from the primary drivers of climate change (e.g., clouds, greenhouse gases, and aerosols). Figure 1 obtained from Stephens et al. (2012) shows how energy is distributed throughout the Earth-atmosphere system. Radiative fluxes in this figure were calculated using BUGSrad (the same algorithm used here) using information from the vertically resolved observations of clouds from CloudSat and MODIS. With the added dimension of the vertically resolved cloud and aerosol properties the global mean estimates from this work provided an improved estimate of the surface Earth's radiation budget for this relatively short time-series of A-Train observations. The uncertainties on the radiative fluxes shown in Figure 1 set benchmarks for the expected accuracy of the retrieval scheme described here. By applying BUGSrad to high spatial resolution (typically 1-km) data spanning multiple decades using the radiatively consistent ORAC retrieval scheme we will advance our understanding of the role of cloud and aerosol feedbacks on the climate system thereby aiming to improve model projections of future climate change.

2 Algorithm

2.1 Description

BUGSrad is based on the two-stream approximation and correlated- k distribution methods of atmospheric radiative transfer. The basis of the algorithm is the same as that described by Fu and Liou (1992). It is applied to a single-column atmosphere for which the cloud and aerosol layers are assumed to be plane-parallel. Cloud and aerosol properties retrieved using ORAC are ingested into BUGSrad to compute both shortwave and longwave radiative fluxes for the top and bottom of atmosphere. The algorithm uses 18 bands that span the entire electromagnetic spectrum to compute the broadband flux. The bands of integration and primary absorbers within each band are shown in Table 1. In total, 6 bands are used for shortwave and 12 bands are used for longwave radiative flux calculations.

The BUGSrad code was initially developed for use in the CAM (Community Atmosphere Model) general circulation model (Collins et al., 2004). The code has also been applied to satellite data [see Henderson et al. (2013)] and has demonstrated excellent agreement between CloudSat/MODIS with CERES measured broadband fluxes. Here, we employ a similar strategy as that adopted by Henderson et al. (2013) to compute the top and bottom of atmosphere broadband radiative fluxes using the Level 2 cloud and aerosol optical properties from (A)ATSR, MODIS, and SEVIRI instruments. In addition, the Photosynthetic Active Radiation (PAR) which designates the spectral range of solar radiation between 400 and 700 nm has been extracted from the first shortwave band in BUGSrad using a similar methodology as that described in Su et al. (2007). PAR has wide usage across multi-disciplinary research topics, some of which include: agriculture and forestry for crop growth models and oceanography for the retrieval of euphotic depth in the ocean to name a couple.

The primary inputs to BUGSrad are the particle effective radius, optical thickness, solar zenith angle, visible and near-infrared surface albedo, surface temperature, total solar irradiance measurements from the SOHO (Solar and Heliospheric Observatory) and SORCE (Solar Radiation and Climate Experiment) instruments, and



vertical profiles of temperature, humidity, and ozone. Per default an aerosol optical depth of 0.05 is used. However an option has been established which facilitates the utilization of Aerosol_cci Level-2 or NASA MODIS Level-2 aerosol data as input. Here, constant values are used for well-mixed RITS (Radiatively Important Trace Species) gases which include $\text{CH}_4 = 1.8$ ppm, $\text{N}_2\text{O} = 0.26$ ppm, and $\text{CO}_2 = 380$ ppm. Constant values are used because spatial variations in these gases tend to be small (less than 5% typically between land and ocean observations). Separate offline calculations of the outgoing longwave flux were computed by changing the constant values by $\pm 5\%$. This yielded a maximum OLR change of approximately 0.3 W/m^2 by combining variances from all trace-gases. Therefore, we do not expect typical spatial variations in these RITS gases to influence the accuracy of the retrieval substantially.

Figure 2 shows the processing chain needed to run the BUGSrad algorithm within ORAC. Pixels are processed at the instrument resolution (1-km for (A)ATSR and MODIS, 3-km SEVIRI). Pixels are deemed to be overcast or clear depending on the value of the cloud mask specified in the primary cloud file. Radiative fluxes are calculated twice for each pixel: the first time using the ingested cloud/aerosol properties to obtain the observed flux and a second time by assuming the pixel is cloud/aerosol-free to obtain the clear-sky flux in the absence of clouds and aerosols. The advantage of the second retrieval makes it possible to calculate cloud (CRE) and aerosol (ARE) radiative effects whereby $CRE = F_{clear} - F_{observed}$ is the difference in outgoing top of atmosphere broadband radiative flux between clear (F_{clear}) - and all-sky conditions ($F_{observed}$).

The physical thickness of clouds is a required input into the radiation scheme. Cloud base height is calculated from the cloud top height, optical depth, and effective radius applied a semi-adiabatic profile as described in (Meerkotter and Zinner, 2007) using the following equation

$$CBH = CTH - \sqrt{\frac{CWP}{f_{ad} \Gamma(T, P)}}, \quad (1)$$

where, CBH is cloud base height, CTH is cloud top height, Γ is the adiabatic rate of increase of liquid water content with respect to height which weakly depends on temperature and pressure for shallow boundary layer clouds (Wood, 2006), CWP is the cloud water path derived separately for water clouds following (Stephens, 1978) as

$$LWP = \frac{2 \tau_{cld} r_e}{3}, \quad (2)$$

and ice clouds following (Fu and Liou, 1992) as

$$IWP = \frac{\tau_{cld}}{[a + b/2r_e]}, \quad (3)$$

where, τ_{cld} is cloud optical depth, r_e is effective radius, $a = -6.656e-3$, and $b = 3.686$. For deeper convective type clouds the variations in temperature and pressure throughout the cloud layer can result in large variations in $\Gamma(T, P)$. Therefore, the temperature and pressure at the middle of the cloud layer is used to represent the mean state of the cloud via a two step approach. Cloud top temperature and pressure are used to determine cloud thickness as a first guess using equation 1. Then the temperature and pressure for the middle of the cloud layer is computed from the first guess cloud thickness using a pseudo adiabatic lapse rate of 5.5 K/km and hydrostatic approximation to obtain pressure from cloud top to the location at the middle of the cloud layer. Cloud base height and thickness is then re-calculated using the corrected temperature and pressure from the middle of the cloud layer. When the temperature is less than 217 K $\Gamma(T, P)$ becomes very small causing highly uncertain estimates of cloud base height. To reduce the uncertainty of this quantity values of $\Gamma(T, P)$ are required to be larger than 0.05; and if smaller the value of $\Gamma(T, P)$ is set to equal 0.05. This method has been used to compute cloud base height from VIIRS (Visible/Infrared Imager/Radiometer Suite) observations (Tsugawa, 2011) and found to agree well against ceilometer observations of convective clouds (Meerkotter and Zinner, 2007).



Incoming shortwave radiation flux at the top of the atmosphere is determined using the total solar irradiance data measured from SOHO and SORCE as shown in figure 3. Daily mean broadband flux measurements are acquired from http://disc.sci.gsfc.nasa.gov/SORCE/data-holdingsusingSOR3TSID_v017. In order to make a continuous time series of the data two steps are required, first employ a bi-linear interpolation scheme to fill missing data from surrounding observations and 2) bias correct the SOHO measurements to match SORCE. The observations are far more stable than they are accurate. As a result, the bias correction method incurs very little uncertainty on the overall time series. The described method we apply above to produce CERES TOA shortwave fluxes is the same as that described in Loeb et al. (2009).

Surface properties are obtained from the preprocessing "alb" file which contains black-sky albedo (ρ_{0d}), white-sky albedo (ρ_{dd}), and emissivity (emis_data) at for multiple bands across the shortwave and longwave spectrums. Surface properties are obtained from the MODIS BRDF (MCD43A1) product which are passed through the ORAC pre-processor and finally to the broadband product. Linear interpolation method is used to fit the surface albedo and emissivity values to the centre of each BUGSrad band. It is noteworthy that if only heritage channels are used in the pre-processor the treatment of the surface albedo will be less accurate because fewer bands are used to do the interpolation. We therefore, highly encourage users to run the pre-processor using the following channels: $n_channels=20$ and $channel_ids=1,2,3,4,5,6,7,20,24,25,27,28,29,30,31,32,33,34,35,36$.

2.2 Validation

Preliminary validation of the top of atmosphere fluxes is examined through comparison with the broadband radiometer on GERB (Geostationary Earth Radiation Budget) MSG-2 (Meteosat Second Generation). Comparisons are made with the GERB ARG (Average Rectified Geolocated) product that is produced at a temporal sampling rate of 15 minutes with a spatial resolution at the sub-satellite point of 44.6 km (N-S) by 39.3 km (E-W). Figure 4 shows a section of the AATSR orbit off the coast of Africa. The image shows three key conditions: 1) deep convective clouds in the north with lower 11 micron brightness temperature, 2) clear-sky pixels in the middle, and 3) patchy cumulus in the south. The top of atmosphere outgoing longwave flux and all-sky albedo (computed from the reflected shortwave flux) is retrieved using BUGSrad and compared to the observations from GERB. GERB observations are collocated in space with AATSR, the two sets of observations are separated in time by about 8 minutes. Spatial patterns of the radiative fluxes between products show consistent agreement with the exception of differences due to different spatial resolutions of each sensor. Figure 5 shows the results of the pixel-scale values in OLR and all sky-albedo. Differences in OLR are within 3 W/m^2 . This is an acceptable bias since the uncertainty on the GERB measured OLR is 1% or roughly the same amount based on typical OLR values Clerbaux et al. (2009). Bias in the all-sky albedo is much larger by comparison at 13% and outside of the normal GERB measurement uncertainty. We are currently investigating the nature of the bias as it may be related to the treatment of surface albedo in the model.

2.3 Uncertainties

The uncertainty of the flux products is derived from comparison of the flux products with SURFRAD sites (see Figure 7). The dark blue values are the values for the standard BUGSRAD setting, while light blue and red show different configurations of the Fu Liou scheme.

Figure 8 shows an example scene over southern Europe and northern Africa for TOA upwelling longwave and BOA downwelling shortwave fluxes and corresponding uncertainties. The data is from AATSR for 2008/08/15.



3 Science applications

3.1 Cloud & Aerosol Radiative Effects

It is important to quantify cloud and aerosol radiative effects because of their strong influence on climate change. Figure 6 shows the global distributions of cloud and aerosol radiative effects over three months (June, July, and August) of AATSR observations during 2008. Radiative effects are the difference between the observed flux and that of a clear-sky atmosphere (no clouds or aerosols); e.g. $CRE = F_{clr} - F_{obs}$, where F_{clr} is the top of atmosphere clear-sky flux and F_{obs} is the retrieved flux for the observed cloud or aerosol properties. Cloud radiative effect is computed from cloudy pixels while aerosol direct radiative effect is computed from cloud-free pixels, each weighted by their frequency of occurrence. Data is aggregated and statistics are computed over into $1^\circ \times 1^\circ$ regions.

The estimation of cloud radiative effect using this product shows promising results and can be summarised in the following points: 1) shortwave cloud albedo effect is largest in regions dominated by low-level clouds (such as the mid-latitude storm tracks and stratocumulus dominated regions), 2) longwave cloud effect is largest in regions dominated by thick high-level clouds (such as across the Intertropical Convergence Zone and mid-latitude storm tracks), and 3) aerosol direct shortwave effect is clearly observed in the wake of sulphur emissions from Hawaii and dust plumes transported off the coast of Africa. Application of this new product to study long-term changes in cloud and aerosol radiative effect is being planned for assessment after production of L3 data.

4 Discussion and Summary

Implementation of BUGSrad to compute broadband radiative fluxes has been incorporated into CC4CL. The initial results are promising. The radiative fluxes between AATSR-BUGSrad and GERB agree within the expected retrieved uncertainty for clear-sky conditions (i.e., $\pm 3 \text{ W/m}^2$). Further direct testing between MODIS - ORAC retrieval and CERES observations is ongoing work. Quantitative cloud radiative effect estimates agree with past studies (see Ramanathan et al., 1989; Thomas et al., 2013). For the aerosol, note, aerosol retrieved over bright deserts actually dim the all-sky albedo, thereby causing a positive forcing. Given the uncertain nature of the treatment of the surface albedo at this time, we are hesitant to quantify the extent of these positive radiative effect regions. Further, the aerosol direct effect shows a noticeable spatial pattern in the aerosol wake of the island of Hawaii which may be produced by the relatively higher aerosol optical depths in that region. These results support potential scientific applications where these retrievals will be needed to quantify the radiative impacts of point-source pollution plumes.

The algorithm, being highly adaptable, can be applied to a variety of visible and near infrared passive instruments, thereby providing numerous opportunities to characterise the uncertainty of the forward model and provide the ability to study cloud/aerosol radiative impacts from a host of sensors. This project has been thoroughly nested within the aerosol and cloud_cci project teams, with in-person representation at their progress meetings since the beginning of the project. All computer codes produced thus far can be found in the CC4CL repository (<http://proj.badc.rl.ac.uk/orac>), making them accessible to the cloud_cci development team. The close interaction has allowed the project to provide some input to ongoing ECV development, such as a bug in the treatment of ECMWF re-analyses that was identified because of inconsistent TOA fluxes.

Interaction with the broader CCI program has been through the collocation meeting and AeroSAT workshop held at ESRIN in September and October this year, where there was some interest in using the PAR product to estimate primary production as discussed by Adam Povey. TOA fluxes were applied to an aerosol-cloud interaction study through collaboration with David Neubauer of ETH, Zurich. Results were reported in a poster at AEROCOM by David Neubauer and an oral presentation at the AeroSat workshop by Matthew Christensen. Fluxes were examined as a function of aerosol loading using AATSR observations and compared



to ECHAM6 HAM2 model data.

4.1 Future Algorithm Developments

The most immediate task is to further validate the radiative flux code against CERES observations and ground-based radiometers (with the assistance of cloud_cci collaborators at the Free University of Berlin). The code's accuracy will also be assessed by evaluating the impact of using a different radiative transfer code, such as that proposed in Edwards and Slingo (1995). Development thus far has concentrated on the ORAC algorithm as it is used in both the aerosol and cloud_cci projects, utilising its preprocessing to provide auxiliary information (such as interpolating ECMWF re-analyses). It must be ensured this is appropriate when processing aerosol_cci data produced with other algorithms. In the longer term, as the current code is rather computationally expensive, it will be investigated if efficiencies can be made or if an offline method of calculation (i.e. look-up tables) is necessary.

Table 1: Listed are the bands used to compute the correlated-k coefficients and primary absorber for each band.

waveband	primary absorber
Shortwave	
200 – 689 nm	O ₃
689 – 1299 nm	H ₂ O
1299 – 1905 nm	H ₂ O
1299 – 2500 nm	H ₂ O
2500 – 3509 nm	H ₂ O
3509 – 4000 nm	H ₂ O
Longwave	
4.5 – 5.2 μ m	H ₂ O
5.2 – 5.8 μ m	H ₂ O
5.8 – 7.1 μ m	H ₂ O
7.1 – 8.0 μ m	H ₂ O, CH ₄ , N ₂ O
8.0 – 9.1 μ m	H ₂ O, CH ₄ , N ₂ O
9.1 – 10.2 μ m	O ₃ , H ₂ O
10.2 – 12.5 μ m	H ₂ O
12.5 – 14.9 μ m	H ₂ O, CO ₂
14.9 – 18.5 μ m	H ₂ O, CO ₂
18.5 – 25.0 μ m	H ₂ O
25.0 – 36.0 μ m	H ₂ O
36.0 – μ m	H ₂ O

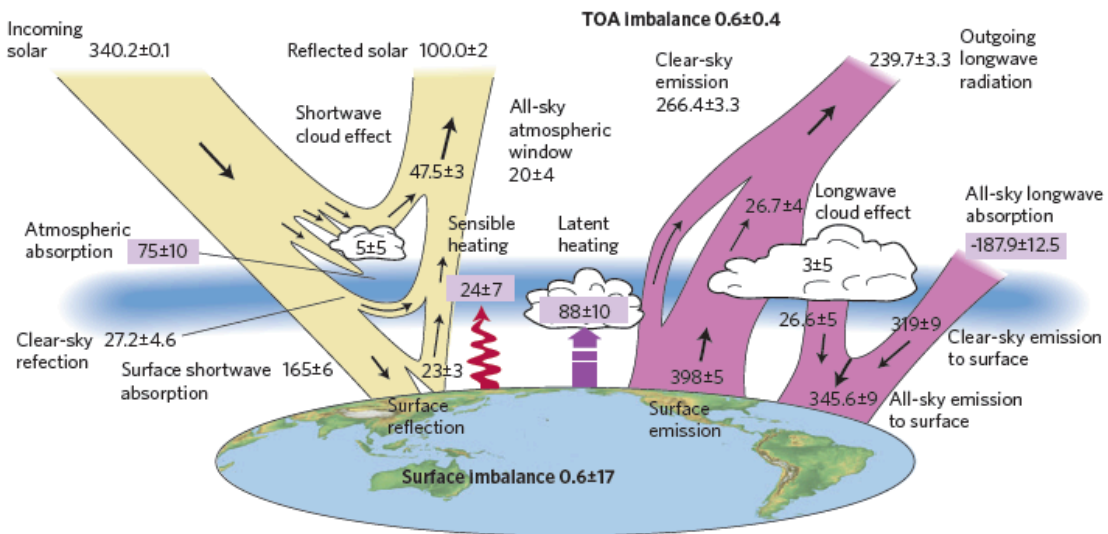


Figure 1: The global annual mean energy budget of Earth for the approximate period 2000 – 2010. All fluxes are in W/m^2 . Solar fluxes are in yellow and infrared fluxes in pink. The four flux quantities in purple-shaded boxes represent the principal components of the atmospheric energy balance. Same figure shown in Stephens et al. (2012)

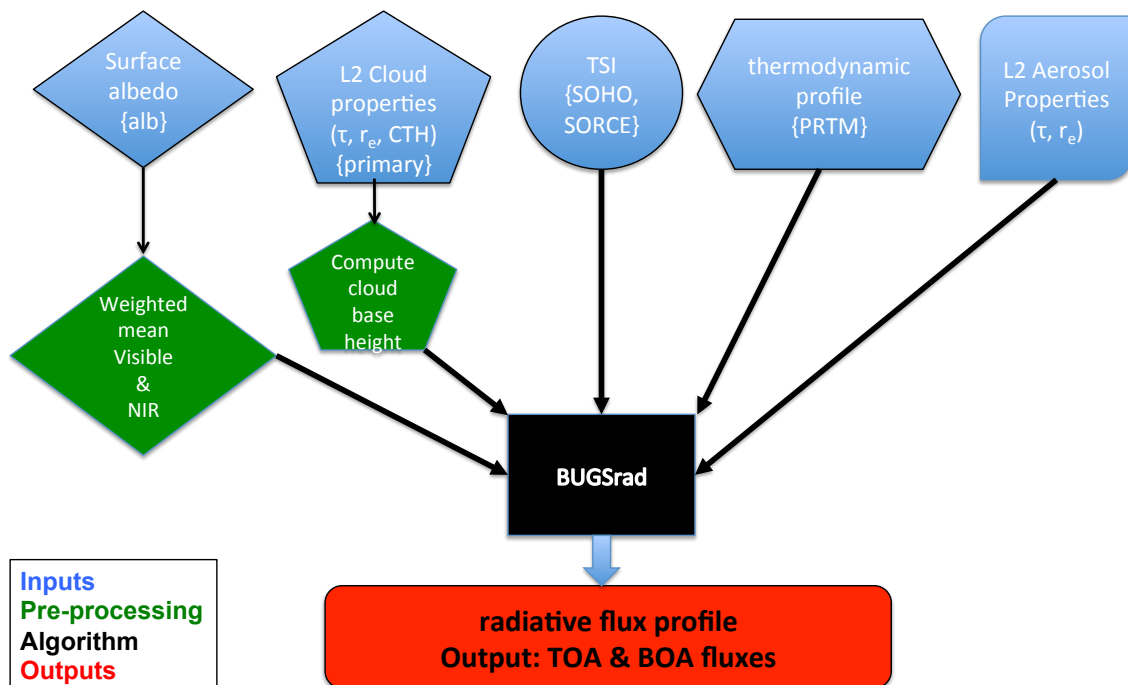


Figure 2: Flow chart of input (blue) and pre-processing variables (green) required to run the BUGSrad algorithm (black) for the output (red) radiative fluxes at the top (TOA) and bottom (BOA) of the atmosphere. Files associated with standard CC4CL output are shown in brackets. Cloud and aerosol optical depth (τ), cloud and aerosol effective radius (r_e), and cloud top height (CTH) are required to run BUGSrad.

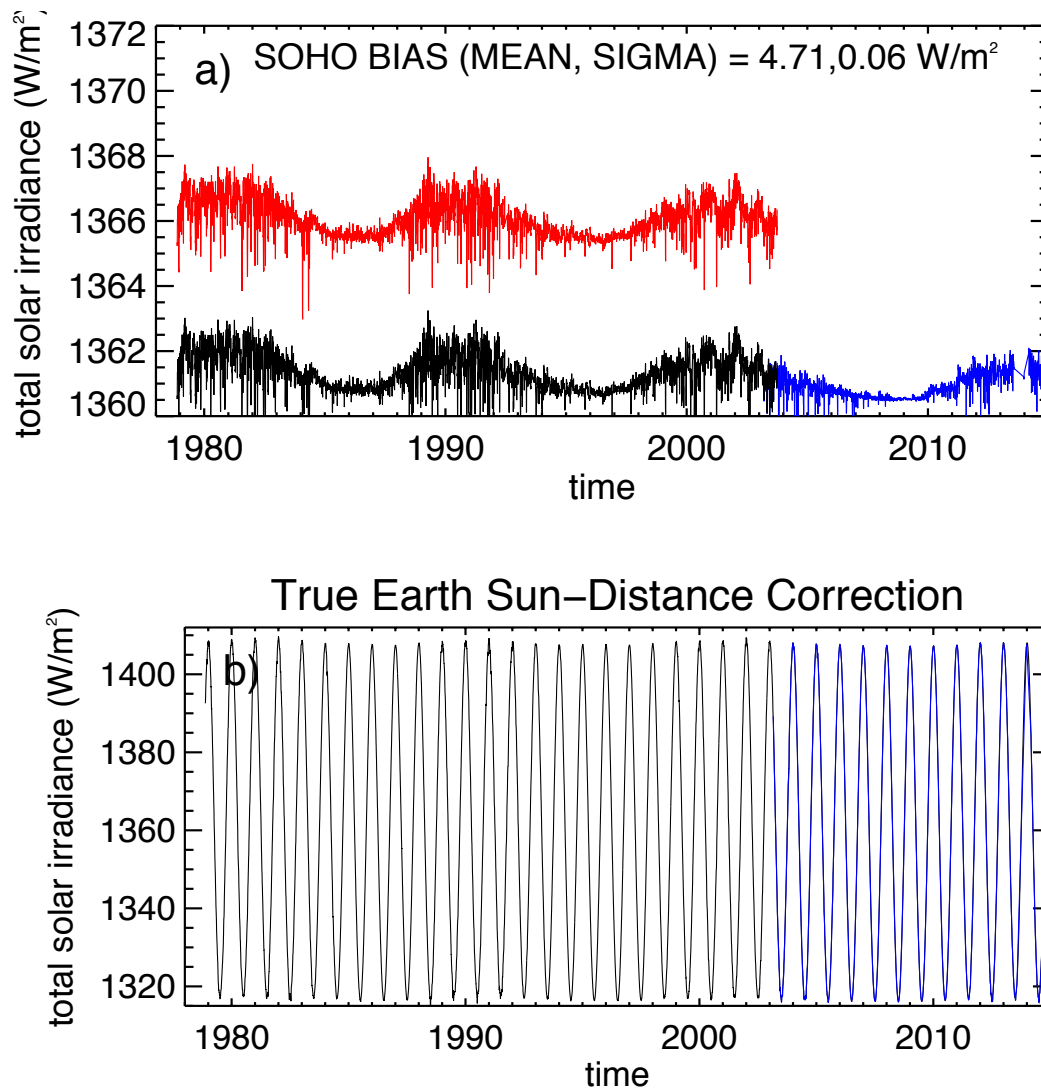


Figure 3: Total solar irradiance (tsi) as measured above the top of atmosphere using SOHO (red; black bias corrected) and SORCE (blue) observations. A bias of approximately 4 W/m^2 is applied to SOHO observations to make a continuous time-series. Total solar irradiance data is corrected (b) based on true earth-sun distance as described by equation (2).

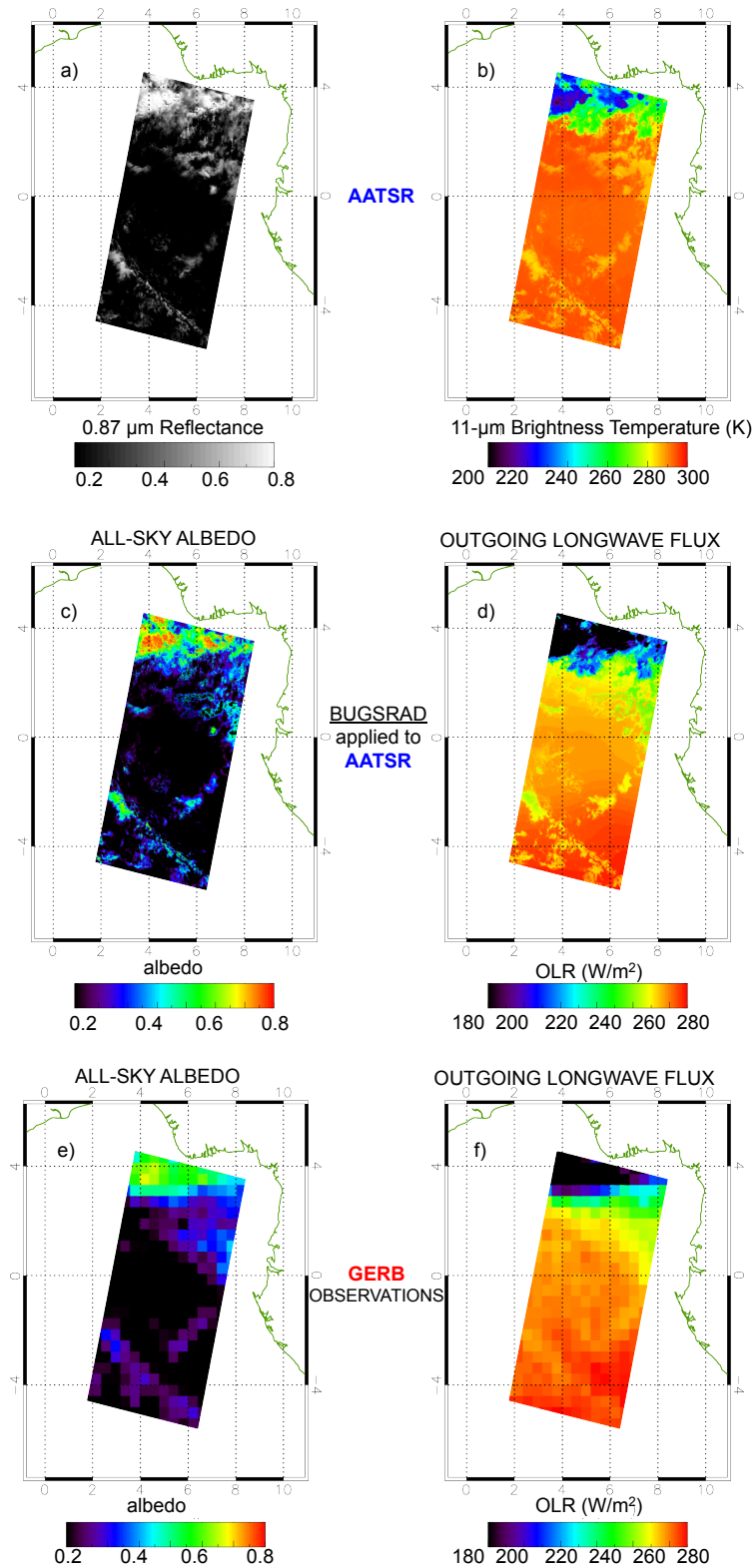


Figure 4: Section of AATSR orbit on 20th of June 2008 off the coast of Africa of the a) 0.87 μm reflectance, b) 11 μm brightness temperature. Retrievals are applied to BUGSrad to produce the top of atmosphere c) all-sky albedo and d) outgoing longwave flux at 1-km resolution. The e) all-sky albedo and f) outgoing longwave fluxes from GERB data are collocated to the AATSR instrument.

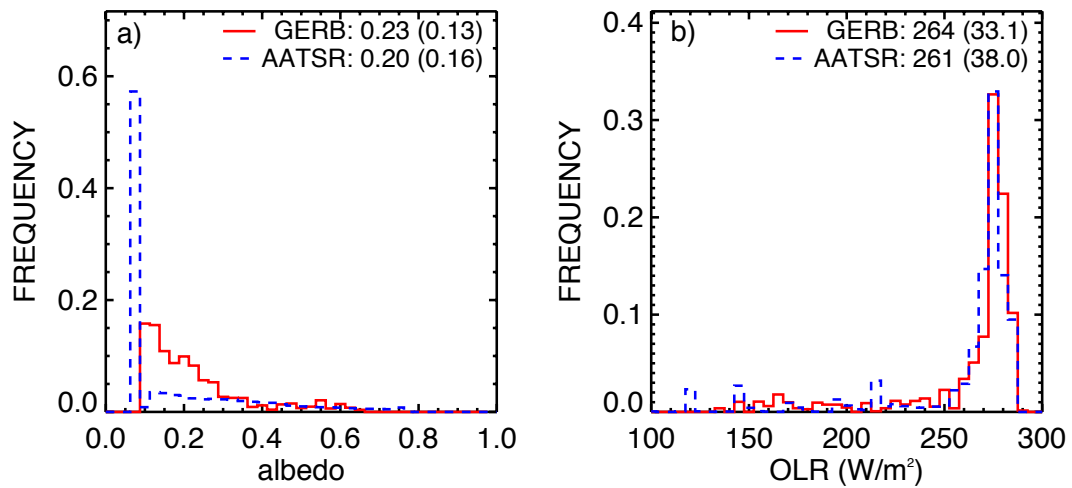


Figure 5: Histogram of top of atmosphere a) allsky-albedo and b) outgoing longwave radiation retrievals shown in Figure 3 for GERB (red) and AATSR (blue) observations. Means and standard deviations (in parenthesis) are calculated from all 1-km pixels for the section of the granule shown in Figure 3.

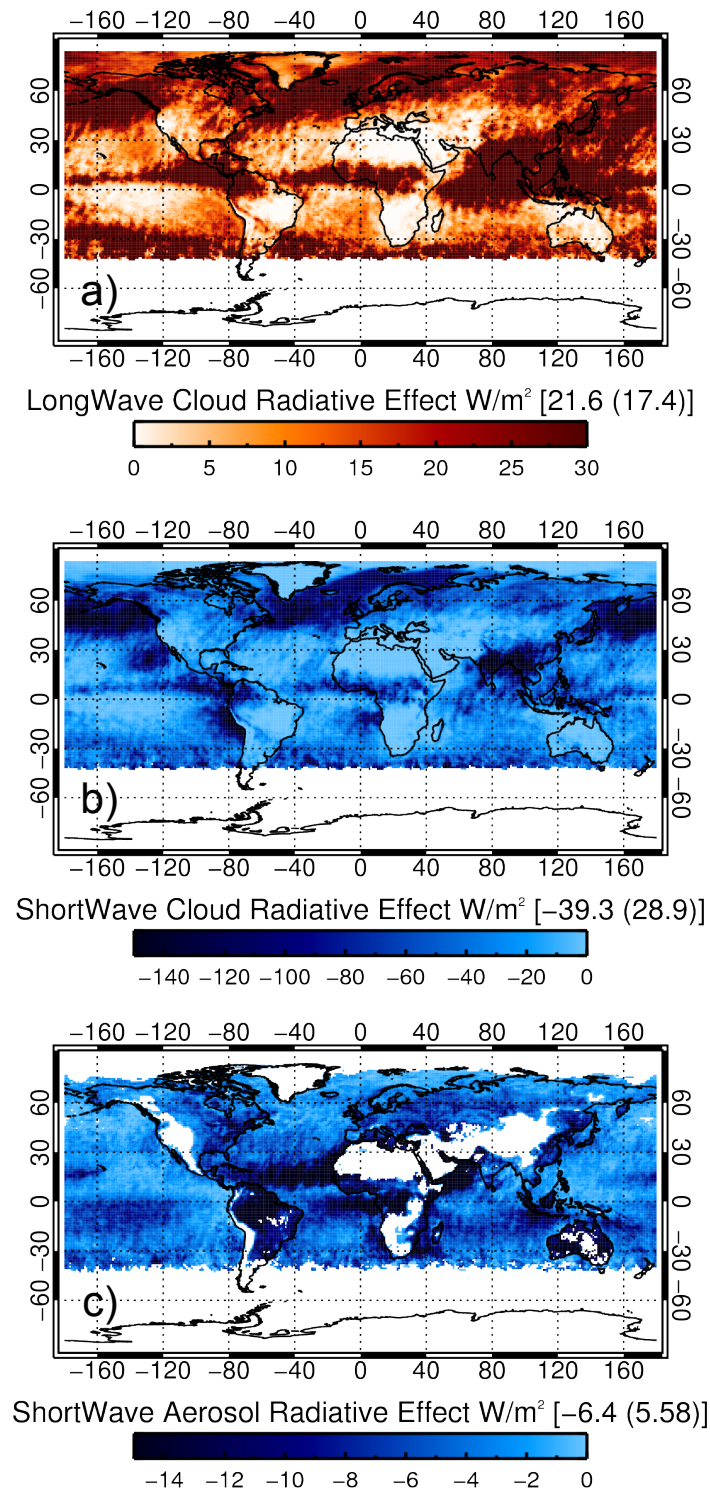


Figure 6: Cloud radiative effect $CRE = F_{clear} - F_{observed}$, the difference in outgoing top of atmosphere broadband radiation between clear- and all-sky conditions in the long and shortwave (a and b, respectively). Global mean values and standard deviations weighted by latitude are provided in brackets. The same, but for a first approximation of the c) aerosol radiative effect.

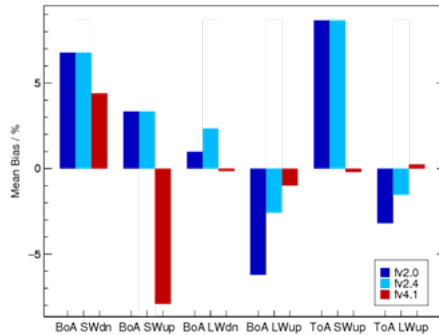


Figure 7: The dark blue values are the values for the standard BUGSRAD setting. Light blue and red show different configurations of the Fu Liou scheme.

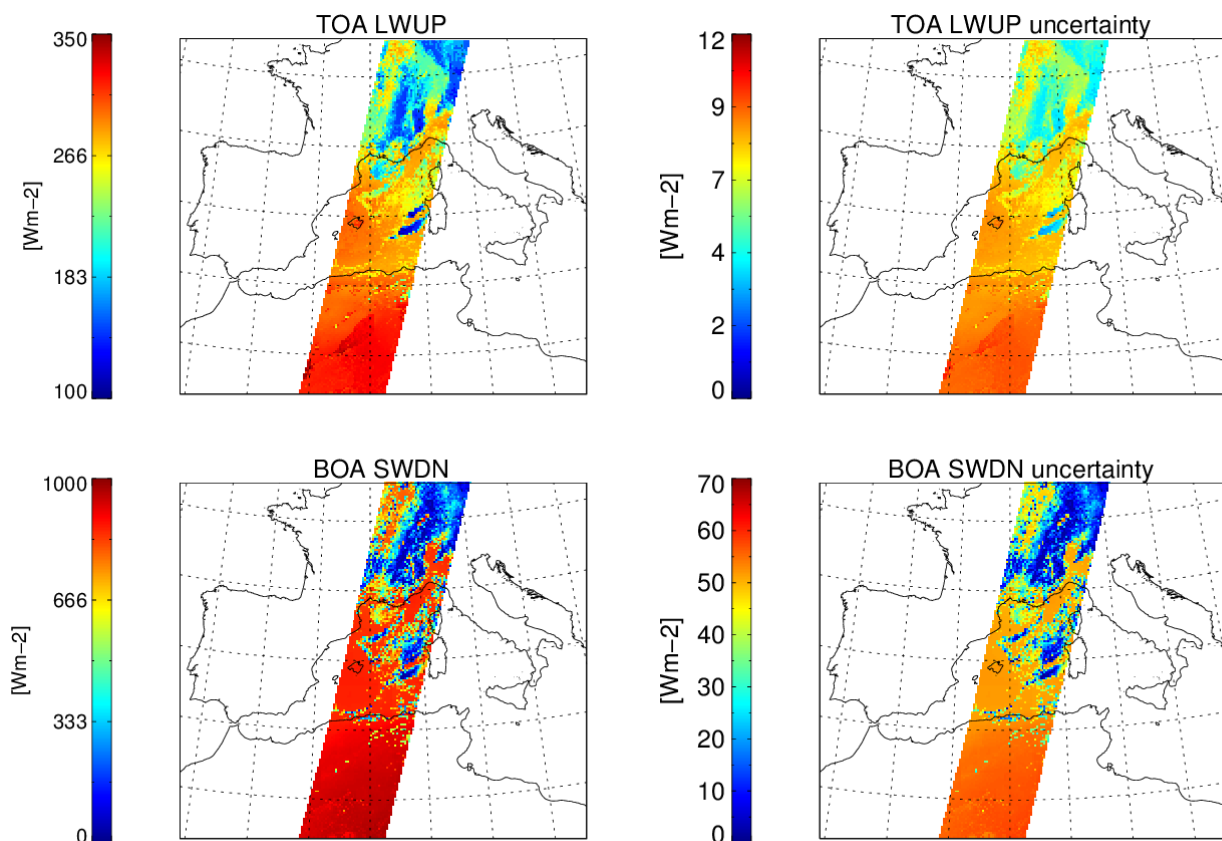


Figure 8: Example scene over southern Europe and northern Africa for TOA upwelling longwave and BOA downwelling shortwave fluxes and corresponding uncertainties. The data is from AATSR for 2008/08/15.



References

- Clerbaux, N., Russell, J., Dewitte, S., Bertrand, C., Caprion, D., De Paepe, B., Gonzalez Sotelino, L., Ipe, A., Bantges, R., and Brindley, H. (2009). Comparison of gerb instantaneous radiance and flux products with ceres edition-2 data. *Remote Sensing of Environment*, 15:102–114. doi:10.1016/j.rse.2008.08.016.
- Collins, W., Rasch, P., Boville, B., Hack, J., McCaa, J., Williamson, D., Kiehl, J., Briegleb, B., Blitz, C., Lin, S., Zhang, M., and Dai, Y. (2004). Description of the ncar community atmosphere model (cam3). technical report ncar/tn- 464+str. *National Center for Atmospheric Research*. Boulder, Colorado 80307-3000, 226 pp.
- Edwards, J. M. and Slingo, A. (1995). Studies with a flexible new radiation code. I: Choosing a configuration for a large-scale model. *Quarterly Journal of the Royal Meteorological Society*, 122:689–719.
- Fu, Q. and Liou, K. N. (1992). On the correlated k-distribution method for radiative transfer in nonhomogeneous atmospheres. *J. Atmos. Sci.*, 49:2153–2170.
- Henderson, D. S., L'Ecuyer, T., Stephens, G., Partain, P., and Sekiguchi, M. (2013). A Multisensor Perspective on the Radiative Impacts of Clouds and Aerosols. *Journal of Applied Meteorology and Climatology*, 52:853–871.
- Loeb, N., Wielicki, B., Doelling, D., Smith, G., Keyes, D., Kato, S., Manalo-Smith, N., and Wong, T. (2009). Toward optimal closure of the earth's top-of-atmosphere radiation budget. *J. Climate*, 22:748–766. doi: <http://dx.doi.org/10.1175/2008JCLI2637.1>.
- Meerkotter, R. and Zinner, T. (2007). Satellite remote sensing of cloud base height for convective cloud fields: A case study. *Geophys. Res. Lett.*, 34, L17805. doi:10.1029/2007GL030347.
- Ramanathan, V., Cess, R., Harrison, E., Minnis, P., Barkstrom, B., Ahmad, E., and Hartmann, D. (1989). Cloud-radiative forcing and climate: Results from the earth radiation budget experiment. *Science*, 243:57–63. DOI: 10.1126/science.243.4887.57.
- Stephens, G., Li, J., Wild, M., Clayson, C., Loeb, N., Kato, S., L'Ecuyer, T., Stackhouse, P., Lebsock, M., and Andrews, T. (2012). An update on earth's energy balance in light of the latest global observations. *Nature Geoscience*, 5:691–696. DOI: 10.1038/NGEO1580.
- Stephens, G. L. (1978). Radiation profiles in extended water clouds. ii: Parameterization schemes. *J. Atmos. Sci.*, 35:2123–2132.
- Stephens, G. L., Gabriel, P. M., and Partain, P. T. (2001). Parameterization of Atmospheric Radiative Transfer. Part I: Validity of Simple Models. *Journal of the Atmospheric Sciences*, 58(22):3391–3409.
- Su, W., Charlock, T. P., Rose, F. G., and Rutan, D. (2007). Photosynthetically active radiation from Clouds and the Earth's Radiant Energy System (CERES) products. *Journal of Geophysical Research — Biogeosciences*, 112(G02):022.
- Thomas, G. E., Chalmers, N., Harris, B., Grainger, R. G., and Highwood, E. J. (2013). Regional and monthly and clear-sky aerosol direct radiative effect (and forcing) derived from the GlobAEROSOL-AATSR satellite aerosol product. *Atmospheric Chemistry and Physics*, 13(1):393–410.
- Tsugawa, R. (2011). National polar-orbiting operational environmental satellite system (npoess) viirs cloud base height algorithm theoretical basis document (atbd). Goddard Space Flight Center, Greenbelt, Maryland, [Available online at http://npp.gsfc.nasa.gov/sciencedocs/2015-06/474-00045_VIIRS_Cloud_Base_Height_ATBD_Rev-_20110422.pdf].



Wood, R. (2006). Relationships between optical depth, liquid water path, droplet concentration, and effective radius in adiabatic layer cloud. University of Washington, 3 pp. [Available online at http://www.atmos.washington.edu/~robwood/papers/chilean_plume/optical_depth_relations.pdf].